Article

Countermanding Perceptual Decision-Making

Countermanding Perceptual Decision-Making

Interactive race

Interrupted accumulation

Paul G.
Middlebrooks,
Bram B. Zandbelt,
Gordon D. Logan,
Thomas J. Palmeri,
Jeffrey D. Schall

jeffrey.d.schall@vanderbilt.
edu

HIGHLIGHTS

Monkeys can perform combined perceptual decision-making and countermanding

Prefrontal neurons accumulate evidence, but this accumulation can be interrupted

Interactive race of response accumulators and a stop accumulator explains findings

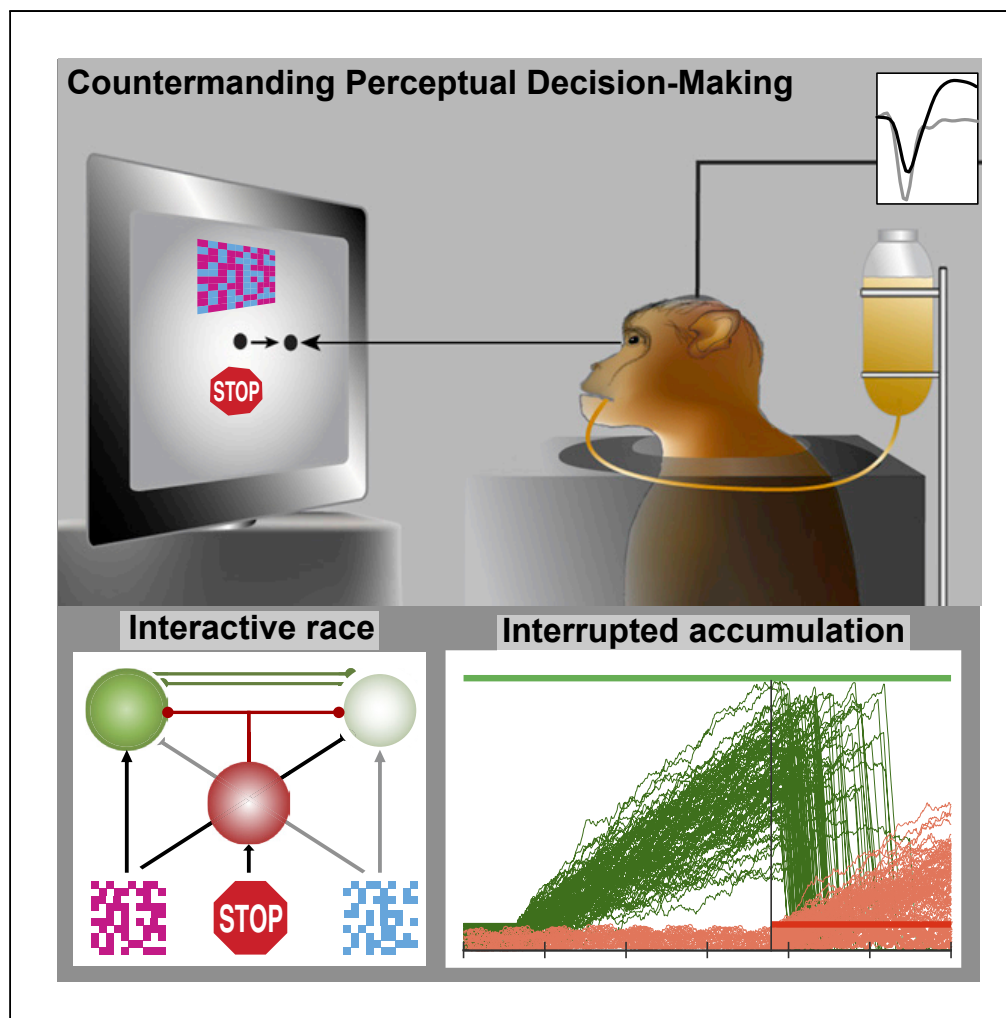Results clarify the circuit logic of brain regions involved in decision-making

Article

Countermanding Perceptual Decision-Making

Paul G. Middlebrooks,[1] Bram B. Zandbelt,[1] Gordon D. Logan,[1] Thomas J. Palmeri,[1] and Jeffrey D. Schall[1,2,*]

SUMMARY

We investigated whether a task requiring concurrent perceptual decision-making and response control can be performed concurrently, whether evidence accumulation and response control are accomplished by the same neurons, and whether perceptual decision-making and countermanding can be unified computationally. Based on neural recordings in a prefrontal area of macaque monkeys, we present behavioral, neural, and computational results demonstrating that perceptual decision-making of varying difficulty can be countermanded efficiently, that single prefrontal neurons instantiate both evidence accumulation and response control, and that an interactive race between stochastic GO evidence accumulators for each alternative and a distinct STOP accumulator fits countermanding choice behavior and replicates neural trajectories. Thus, perceptual decision-making and response control, previously regarded as distinct mechanisms, are actually aspects of a common neuro-computational mechanism supporting flexible behavior.

INTRODUCTION

Perceptual decision-making is commonly studied using two-alternative forced-choice tasks in which one of two responses is produced based on a visual discrimination. Performance is explained by sequential sampling of evidence accumulation, which appear to correspond to the dynamics of particular neurons in sensorimotor brain structures (O'Connell et al., 2018; Ratcliff et al., 2016; Schall, 2019). Response control is commonly studied using stop-signal (countermanding) tasks in which a planned response should be withheld if a stop-signal occurs. Performance is explained by race models of the initiation or cancellation of a response, which correspond to the dynamics of particular neurons in sensorimotor structures (Boucher et al., 2007; Logan and Cowan, 1984; Logan et al., 2015; Verbruggen and Logan, 2009). Neither standard model accounts for performance and neurophysiology of the other task, and it is unknown whether neurons instantiate both processes. Therefore we investigated (1) whether perceptual decisions and response control can be performed concurrently, (2) whether they are accomplished by the same neurons, and (3) whether perceptual decision-making and countermanding can be unified computationally.

RESULTS

Countermanding Choice Performance

Neural spiking was sampled from two macaque monkeys (Br, Jo) performing a task that combined visual decision-making and saccade countermanding. On each trial, a cyan and magenta checkerboard was presented. The color coherence of the checkerboard was varied to influence the choice direction and discrimination difficulty. Monkeys reported the majority color with a saccade to one of two peripheral targets consistently mapped onto each color (Figure 1A). On a minority of trials (~30%), a visual stop-signal was presented at the fixation point after a variable stop-signal delay. On no-stop trials, reinforcement was earned for a correct choice. On stop-signal trials, two outcomes were possible. Reinforcement was earned for canceling the choice saccade. No reinforcement was delivered if the saccade was not canceled. Analysis of performance using the Logan and Cowan (1984) race model provides a measure of the duration of the countermanding process, known as stop-signal reaction time (SSRT) (Verbruggen et al., 2019).

Performance data from each monkey manifest classical features of both the perceptual decision-making and the countermanding tasks (Figures 1B and S1, Table S1). Response times and error rate both increased with difficulty across both color coherence and stop-signal delay (Br: RT: $F(3,59) = 12.10$, $\eta_p^2 = 0.38$, $p < 0.001$; error rate: $F(3,35) = 759$, $\eta_p^2 = 0.50$, $p < 0.001$; Jo: RT: $F(3,62) = 3.78$, $\eta_p^2 = 0.15$, $p = 0.015$; error rate: $F(3,35) = 363$, $\eta_p^2 = 0.49$, $p < 0.001$). Discrimination difficulty manipulated by color coherence had no effect on SSRT (Br: $F(3,16) = 0.86$, $\eta_p^2 = 0.14$, $p = 0.48$; Jo: $F(3,16) = 0.68$, $\eta_p^2 = 0.11$, $p = 0.58$). This pattern of results was replicated in performance collected in separate sessions with monkey Br and with a third monkey (X) (Figure S1, Table S1). Replicating previous findings with macaques and humans (Logan et al., 2014;
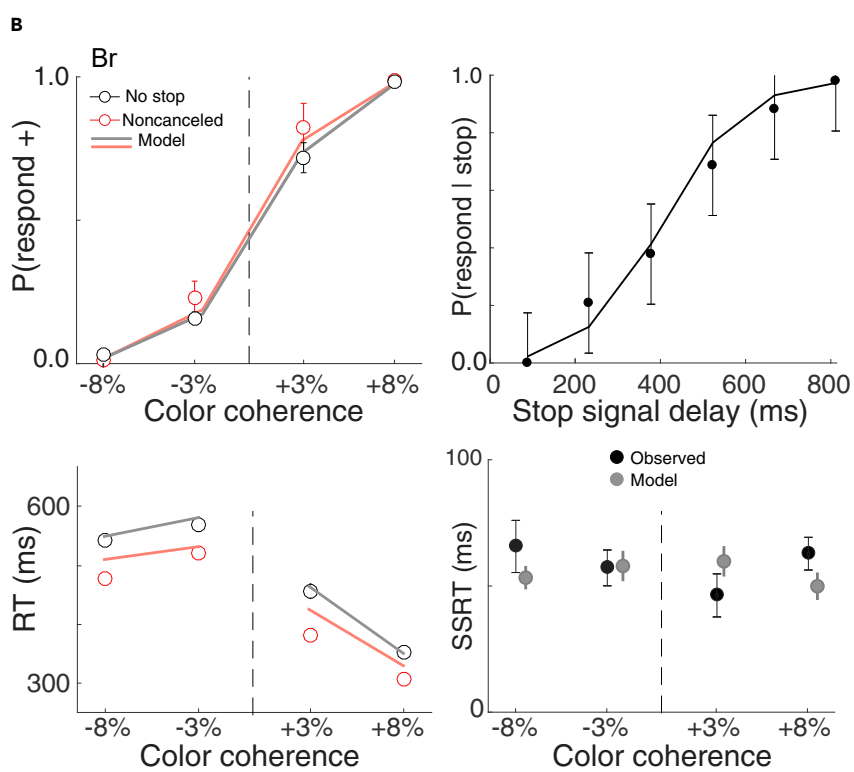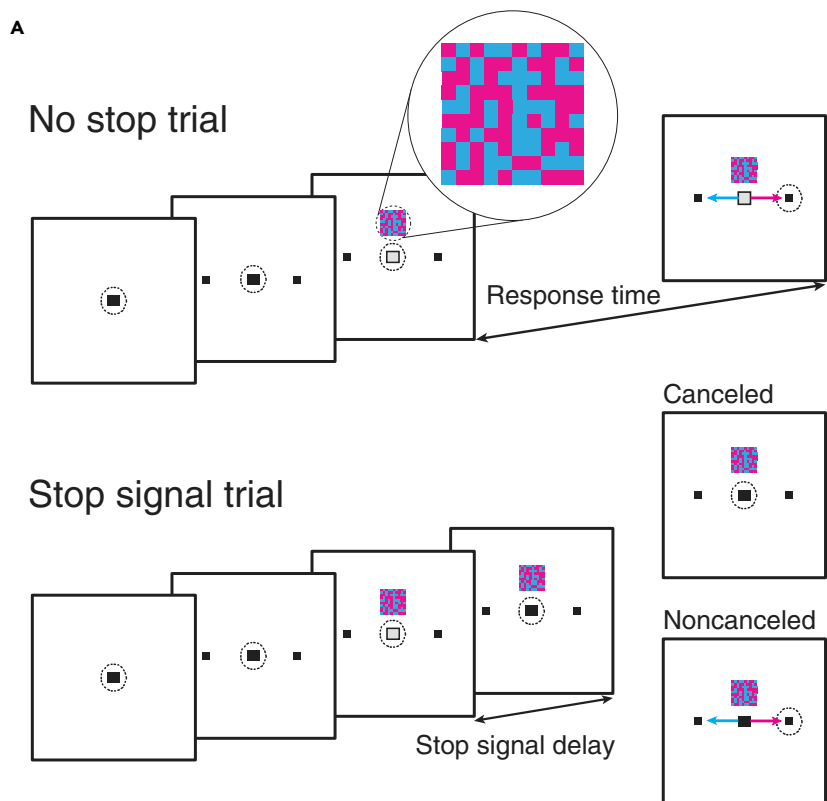
A

B

Figure 1. Perceptual Decision Countermanding Task

(A) No-stop trials (top panel) began by fixating a central spot. After a variable delay, two targets appeared in the periphery. After another variable delay, a 10 × 10 checkerboard choice stimulus (magnified inset) appeared 3° above the fixation spot, while the fixation spot simultaneously disappeared. The checkerboard was composed of variable fractions of cyan and magenta squares. Fluid reward was delivered if monkeys shifted gaze to the target assigned to the majority color. On a minority of trials (stop-signal trials, bottom panel), the fixation spot reappeared after a variable stop-signal delay. Reward was delivered if monkeys canceled the planned saccade.

(B) Performance of monkey Br during neural recordings. Upper left: Mean ± SEM choice probability as a function of color coherence for no-stop (black) and non-canceled (red) trials. Gray and red lines plot values predicted by best fit model. Upper right: Inhibition function averaged across all sessions. Solid line plots the inhibition function predicted by the best fit model. Lower left: Mean ± SEM of response time (RT) as a function of color coherence for correct choice no-stop (black) and non-canceled (red) trials. Non-canceled RT was systematically shorter than no-stop RT, justifying the application of the Logan and Cowan race model. Gray and red lines plot values predicted by the best fit model. Lower right: Mean ± SEM stop-signal reaction time (SSRT) derived from race model as a function of color coherence (black). SSRT did not vary with decision-making difficulty. Mean ± maximum and minimum SSRT predicted by the best fit model (gray).

Middlebrooks and Schall, 2014), perceptual decision-making and response inhibition appear to operate concurrently and efficiently.

Neural Spiking during Choice Countermanding

Patterns of neural spiking sampled in the frontal eye field (FEF), a prefrontal area at the interface of visual decision-making and saccade production (Schall, 2015), also manifest classical features of both the perceptual decision-making and the countermanding tasks (Figures 2 and S2). This report is based on 1,398 neural spiking samples of which 696 were modulated during the task with 206 exhibiting presaccadic ramping activity. Of these presaccadic units, 52% were modulated with the difficulty of the perceptual choice mirroring the evidence accumulation process accounting for the variation of response time (RT) (Figure 2, Table S2), replicating previous observations (Ding and Gold, 2012).

As observed before, when saccades were not canceled, modulation of the presaccadic units was indistinguishable from no-stop trials with equivalent RTs (Figure S2). When choice saccades were canceled, 58% presaccadic units modulated before SSRT in a manner sufficient to control saccade initiation, also replicating previous observations (Hanes et al., 1998; Murthy et al., 2009; Paré and Hanes, 2003) (Table S2).

We now report that when choice saccades were canceled, of the 52% presaccadic neurons modulated with perceptual difficulty, 81% also modulated before SSRT (Table S2). This was observed in well-isolated, single units (Figure S2). Presaccadic ramping neurons in FEF have been identified computationally with the GO process of countermanding (Boucher et al., 2007; Logan et al., 2015) and with evidence accumulation for perceptual decision-making (Ding and Gold, 2012; Purcell et al., 2010, 2012). These results show that evidence accumulation and response inhibition are instantiated concurrently by single neurons in prefrontal cortex.

Neuro-computational Model of Choice Countermanding

To determine how neurally plausible choice and stopping models can be unified, we tested an interactive choice race model consisting of two stochastic accumulators for each response alternative (GO^+, GO^-) plus a STOP accumulator (Figure 3). The two GO units and one STOP unit could accumulate activation and interact in various ways defined by particular parameters. We explored which parameters provided the best fit of the correct and error RT distributions, and the variation of choice accuracy and SSRT across choice difficulty and stop-signal delays. The quality of the fits was evaluated with Bayesian information criteria. This model framework with different types of parameter constraints afforded nested hypothesis testing among several distinct architectures.

We tested three mechanisms of choice nested within the same general model architecture (race ($u = 0$, $\beta_{GO} = 0$), feedforward inhibition ($u > 0$, $\beta_{GO} = 0$), and lateral inhibition ($u = 0$, $\beta_{GO} > 0$) between the GO units) and one mechanism of inhibition from the STOP to the GO units ($\beta_{STOP} > 0$). For each architecture, we also evaluated the quality of the fits for five forms of parameter flexibility (Table S3). (1) To account for asymmetric RT across response alternatives, different baseline values (A_0) were allowed for each GO accumulator. (2) To account for variation in RT as a function of color coherence, the GO accumulation rate (μ_{GO}) was allowed to vary with coherence level, but the values were constrained to be equal for the
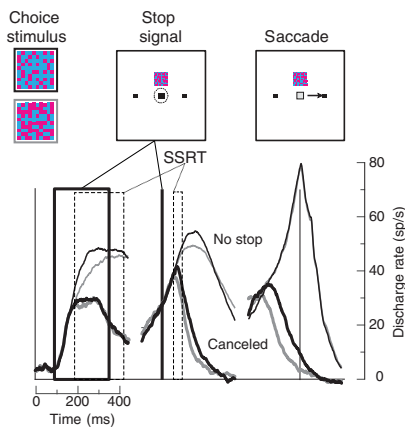
Figure 2. Neural Mechanism of Perceptual Decision Countermanding

Average discharge rates of neurons representing the perceptual decision variable and instantiating race model GO process. Discharge rate is plotted as a function of time relative to presentation of the choice stimulus (left), stop-signal (middle), and saccade (right). The thick lines mark times when stop-signal occurred across trials. Dashed lines mark corresponding SSRT across sessions. On trials with no stop-signal (thin), discharge rates accumulated faster with higher (black) relative to lower (gray) color coherence but reached the same trajectory immediately before saccade initiation. On successfully canceled stop-signal trials (thick), accumulating discharge rates were inhibited before SSRT.

two alternatives. (3) To account for both overall RT asymmetries and variation of RT across color coherence, both baseline values and coherence-dependent accumulation were allowed. (4) To account for asymmetric variation of RT as a function of color coherence, the accumulation rate was allowed to be asymmetric across the two alternatives. (5) To account for both overall RT asymmetries and asymmetric variation of RT as a function of color coherence, asymmetric variation of both baseline values and accumulation rates were allowed. Variation of threshold (A_{θ_GO}) or non-decision time (t_{0_GO}) across conditions did not improve fits to the performance measures. Each architecture accounted well for the combined choosing and stopping performance, with only modest differences in the goodness of fit of the race, feedforward inhibition, and lateral inhibition mechanisms. We regard this as evidence for a robust computational unification of perceptual decision-making and response control because mathematically distinct but functionally similar neural networks can accomplish common functions (Marder et al., 2015).

Performance during neural recordings was fit best by a model with lateral inhibition between the two GO units ($u = 0$, $\beta_{GO} > 0$) and potent inhibition of the GO units by the STOP unit ($\beta_{STOP} >> 0$) (Figure 3, Tables 1 and S3). Asymmetric variation in color coherence difficulty was best accounted for by asymmetric variation in GO unit accumulation rates ($\mu_{GO}^+ \neq \mu_{GO}^-$). Decision error rates were best accounted for by the combination of variation in relative baseline levels and accumulation rates across the two alternatives. Response inhibition was accounted for by late, potent inhibition of the GO units by the STOP unit. The best-fitting models fit the basic performance measures well on average (Figures 1 and S1) and across RT distributions (Figure S3). The interactive choice race model also fit performance collected in separate sessions in monkey Br and in a third monkey (X) (Figure S1, Table S1).

Our approach to testing computational models requires more than fits to performance. The model is supposed to explain what neurons are doing through time. Therefore, we compared the observed times when presaccadic neural activity was interrupted on canceled trials with the times measured in simulated trajectories of GO units with best-fit parameters. As observed in the simpler interactive race model (Boucher et al., 2007; Logan et al., 2015), we found that the STOP unit interrupted the accumulation of the GO units at times corresponding to those measured from the sampled neurons (Figure 3). Hence, these results demonstrate the graceful and robust computational unification of the two primary models of decision-making and response control.

DISCUSSION

Based on the following considerations, we believe the current results can be interpreted more generally. First, the performance measured during neural recordings corresponded to performance measured in other monkeys and four human participants (Middlebrooks and Schall, 2014). Second, the patterns of neural modulation observed corresponded to patterns observed previously in monkeys performing tasks that require only saccade countermanding (Hanes et al., 1998; Paré and Hanes, 2003) or tasks that require only perceptual decision-making (Ding and Gold, 2012; Ratcliff et al., 2003; Roitman and Shadlen, 2002). Therefore, the observation that neurons representing the decision variable for a perceptual decision can be countermanded may be regarded as robust. Third, the quality of the fits achieved by this countermanding decision model was comparable with those achieved by previous fits to perceptual decision or to
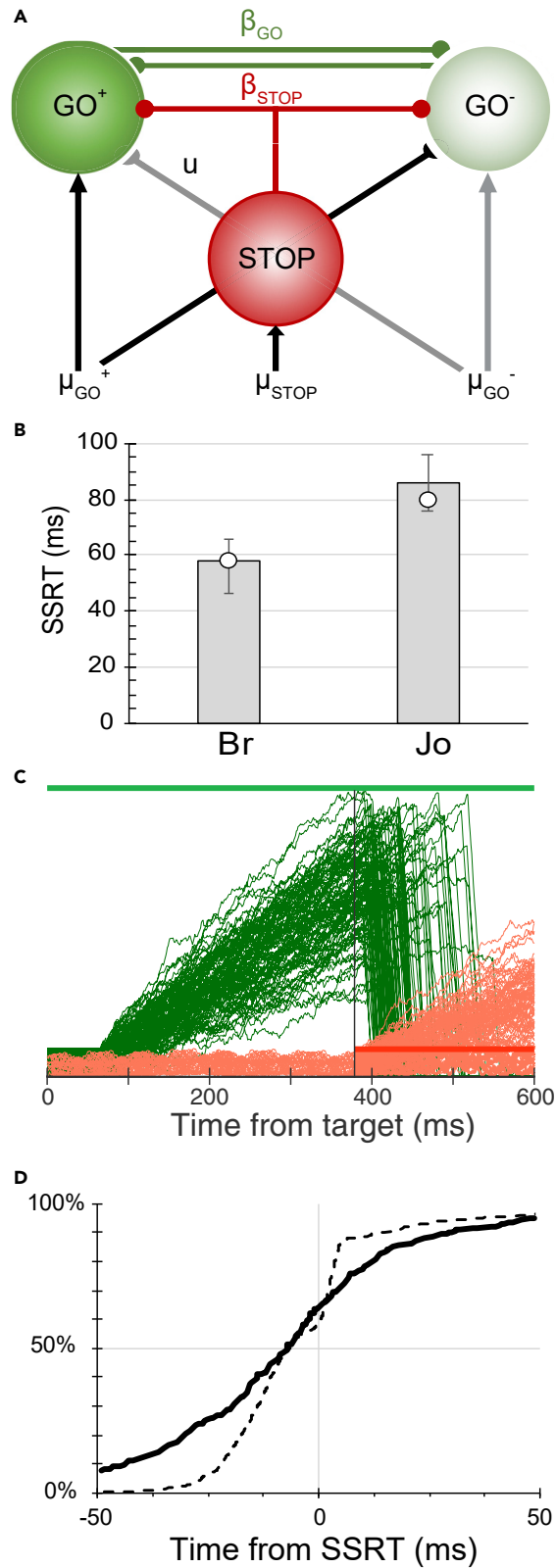
A

B

C

D

Figure 3. Interactive Race Model of Countermanding Perceptual Decision-Making
(A) Model architecture. Alternative decisions are committed when the accumulated activation of one of the GO units reaches a threshold. The accumulation of each GO unit was driven by the evidence supporting each alternative. This accumulation could be reduced by feedforward inhibition proportional to the evidence supporting the other alternative and by lateral inhibition from the other GO unit. Decisions are canceled if the activation of a STOP unit inhibits the GO units. This inhibition arises after a delay, which preserves the stochastic independence of the race finish times.
(B) Comparison of model SSRT for each monkey (circles) with observed SSRT average (bars) and range of minimum and maximum values across sessions (error bars).
(C) Representative trajectories of GO unit and STOP unit on trials with a stop-signal when the response was successfully canceled.
(D) Observed (solid) and simulated (dashed) cancel times.

countermanding performance alone (Boucher et al., 2007; Lo et al., 2009; Logan et al., 2015; Mazurek et al., 2003; Purcell et al., 2010, 2012; Wei and Wang, 2016). Thus, elaborating previous theoretical work (Logan et al., 2014), the interactive race choice countermanding model unifies previously distinct model frameworks.

We sampled some neurons that statistically failed to signal the perceptual decisions. We believe that this is not a consequential observation. Most of these neurons had weak responses to the choice targets, so we surmise that the weak modulation was simply due to a lack of overlap of the most sensitive region of the neuron's response field and the placement of the choice targets. We also sampled neurons that did not modulate before SSRT or at all when choice saccades were canceled. Such diversity in FEF has been found before (Hanes et al., 1998). Further research can elucidate the circuitry of these diverse neurons.

The major general conclusion we draw is that the existence of neurons contributing to both functions concurrently suggests a unity of two cognitive operations that have been regarded as distinct in the visual neuroscience research community. Is this outcome surprising? Was it a foregone conclusion that response selection and the countermanding process interact? This view implies an identification of "perceptual decision-making" with "response selection"; however, other research has highlighted distinctions (e.g., Gold and Shadlen, 2003). Hence, the alternative outcome is that neurons signal the perceptual decision variable but are entirely unaffected by whether or not the movement is canceled. Such a result is likely to be the case in the lateral intraparietal area (LIP) where neurons do not modulate before SSRT (Paré and Dorris, 2011).

Is it reasonable to think that perceptual decision-making and response control are mutually exclusive and would not be performed concurrently? Perhaps the lateralized perceptual decision-making used in this task requires allocation of spatial attention, which corresponds to saccade preparation (Awh et al., 2006). Although spatial attention is certainly necessary for this task, the activity of presaccadic movement neurons in FEF has been dissociated from spatial attention in three different ways. First, visual attention shifts without saccade preparation (Juan et al., 2004). Second, neurons in FEF that mediate visual attention are not connected to saccade motor circuits (Pouget et al., 2009). Third, when attention allocation is signaled with limb movements, the visually responsive neurons in FEF modulate as usual, whereas the movement neurons are suppressed (Thompson et al., 2005). These observations contradict the hypothesis that the activity of FEF movement neurons can be identified with both motor planning and shifting spatial attention.

Conditions in which STOP and GO processes interact strongly have been described (Verbruggen and Logan, 2015). We would also emphasize that the concepts of independence and interaction can have different manifestations at different levels of description. The stochastic independence of GO and STOP processes is central to the Logan and Cowan (1984) race model. However, the discovery that neurons in motor circuits are strongly modulated before SSRT demonstrates clearly that the neural processes instantiating the GO and STOP processes must interact (Hanes et al., 1998; Paré and Hanes, 2003). The interactive race models demonstrate how the appearance of independence and the fact of interaction can be reconciled computationally and mechanistically (Boucher et al., 2007; Logan et al., 2015).

This unification provides a fresh insight into the relationship of deciding and stopping. The STOP unit inhibition parameter was considerably stronger than the GO unit lateral inhibition. Of course, in the race architecture the STOP unit inhibition was infinitely greater than the interaction between GO units. Across all model fits, the STOP unit inhibition averaged 13 orders of magnitude greater than lateral inhibition

Parameters of Best Fit Model		Br Neural Lateral Inhibition		Jo Neural Lateral Inhibition
$A_{0\_GO}^+$		14.9		6.0
$A_{0\_GO}^-$		93.4		18.1
A_{0_STOP}		12.9		9.6
A_{θ_GO}		150.4		39.3
A_{θ_STOP}		13.7		14.6
	COH		COH	
μ_{Go}^+	−8%	0.07	−10%	0.09
	−3%	0.11	−5%	0.16
	3%	0.24	5%	0.19
	8%	0.37	10%	0.22
μ_{Go}^-	−8%	0.31	−10%	0.40
	−3%	0.28	−5%	0.33
	3%	0.24	5%	0.24
	8%	0.16	10%	0.12
μ_{STOP}		0.14		0.13
U		$−7.80 \times 10^{-16}$		−0.058
β_{STOP}		−0.477		−0.410
t_{0_GO}		66		120
t_{0_STOP}		9		13

Table 1. Parameters of Best-Fit Models for Performance during Neural Recording
Activation of units began at a baseline level on each trial drawn from a uniform distribution [0:A_0], which could have different values for the GO^+, GO^-, and STOP units and completed when it reached the respective thresholds (A_{θ_GO}, A_{θ_STOP}). The activation of each GO unit increased with input strength, which varied with color coherence and response direction ($\mu(COH_i, DIR_j)$) and decreased according to lateral inhibition (u) and STOP unit inhibition (β_{STOP}). The activation of the STOP unit (a_{STOP}) increased with input strength (μ_{STOP}). Activation of each unit began after a stimulus encoding non-decision time (t_{0_GO}, t_{0_STOP}). Choice countermanding performance was fit best with lateral inhibition between the GO units, and late potent inhibition of the GO unit, by the STOP unit.

between GO units and 5 orders of magnitude greater than forward inhibition on GO units (Table S3). Moreover, as found earlier (Boucher et al., 2007; Logan et al., 2015), the action of the STOP unit was necessarily delayed to preserve the independence of the finishing times of the racing GO and STOP processes. These model parameters entail that although response inhibition can be conceived as an alternative decision in the model architecture, it functions with dynamics different from the processes producing overt responses. In other words, interrupting a choice is different from executing one among alternative choices.

Our findings confirm a specific linkage in prefrontal cortex between response preparation and perceptual decision-making. This contradicts an earlier conclusion that frontal cortex in rodents does not contribute to evidence accumulation (Hanks et al., 2015), but replicates multiple, previous, independent observations (Ding and Gold, 2012; Purcell et al., 2010, 2012). The existence of neurons in prefrontal cortex instantiating evidence accumulation also provides an explanation for the persistence of perceptual decision-making when posterior cortical areas are inactivated (Katz et al., 2016) and the ability of monkeys to perform the task before posterior parietal neurons acquire the accumulation process (Law and Gold, 2008). Taken together, these results suggest that the evidence accumulation signal reported in parietal cortex is derived from more primary processes occurring in the frontal lobe and perhaps subcortically. This hypothesis would

be verified if inactivation of FEF disrupted performance of perceptual decision-making and countermanding with saccadic eye movements.

Thus, innovative performance, neural signaling, and computational modeling results demonstrate that perceptual decisions and response inhibition are not separate processes but instead just different descriptions of a single process traditionally tested in different modes of operation. Our results elaborate further constraints on the circuit logic of brain regions involved in decision-making.

Limitations of the Study

The conclusions are constrained by the following limitations. First, no inactivation was done to determine whether FEF is necessary for performance of this task. However, lesion (Dias and Segraves, 1999) and inactivation (Wardak et al., 2006) studies have demonstrated that FEF is necessary for saccades produced in more complex conditions including perceptual decision-making during visual search. Also, interpretation of inactivation findings is always limited by questions about the actual extent and efficacy of the inactivation. Second, neural discharges were not sampled in other brain regions known to contribute to performance of this task. We do not know, for example, how neurons in posterior parietal cortex contribute to performance of this combined task given the absence of modulation when saccades are countermanded (Paré and Dorris, 2011). Also, we do not know how the choice stimulus or the stop-signal is encoded from visual processing through task rule, but evidence indicates that this likely involves other prefrontal areas (Xu et al., 2017). Ultimately, this specific task and general approach offers an effective means of assessing the contributions of multiple nodes in the distributed network that supports perceptual decision-making and response control.

METHODS

All methods can be found in the accompanying Transparent Methods supplemental file.

DATA AND CODE AVAILABILITY

All datasets and custom analysis programs will be made available upon request to the Lead Contact, Jeffrey D Schall (jeffrey.d.schall@vanderbilt.edu).

SUPPLEMENTAL INFORMATION

Supplemental Information can be found online at https://doi.org/10.1016/j.isci.2019.100777.

AUTHOR CONTRIBUTIONS

Conceptualization, P.G.M., B.B.Z., G.D.L., T.J.P., and J.D.S.; Methodology, P.G.M., B.B.Z., G.D.L., T.J.P., and J.D.S.; Software, P.G.M., B.B.Z.; Validation, G.D.L., T.J.P., and J.D.S.; Formal Analysis, P.G.M., B.B.Z., and J.D.S.; Investigation, P.G.M., J.D.S.; Writing – Original Draft, P.G.M. and J.D.S.; Writing – Review & Editing, P.G.M., B.B.Z., G.D.L., T.J.P., and J.D.S.; Visualization, P.G.M. and J.D.S.; Supervision, G.D.L., T.J.P., and J.D.S.; Funding Acquisition, G.D.L., T.J.P., and J.D.S.

DECLARATION OF INTERESTS

The authors declare no competing interests.

REFERENCES

Awh, E., Armstrong, K.M., and Moore, T. (2006). Visual and oculomotor selection: links, causes and implications for spatial attention. Trends Cogn. Sci. *10*, 124–130.

Boucher, L., Palmeri, T.J., Logan, G.D., and Schall, J.D. (2007). Inhibitory control in mind and brain: an interactive race model of countermanding saccades. Psychol. Rev. *114*, 376–397.

Dias, E.C., and Segraves, M.A. (1999). Muscimol-induced inactivation of monkey frontal eye field: effects on visually and memory-guided saccades. J. Neurophysiol. *81*, 2191–2214.

Ding, L., and Gold, J. (2012). Neural correlates of perceptual decision making before, during, and after decision commitment in monkey frontal eye field. Cereb. Cortex *22*, 1052–1067.

Gold, J.I., and Shadlen, M.N. (2003). The influence of behavioral context on the representation of a perceptual decision in developing oculomotor commands. J. Neurosci. *23*, 632–651.

Hanes, D.P., Patterson, W.F., and Schall, J.D. (1998). Role of frontal eye fields in countermanding saccades: visual, movement, and fixation activity. J. Neurophysiol. *79*, 817–834.

Hanks, T.D., Kopec, C.D., Brunton, B.W., Duan, C.A., Erlich, J.C., and Brody, C.D. (2015). Distinct relationships of parietal and prefrontal cortices to evidence accumulation. Nature *520*, 220–223.

Juan, C., H., Shorter-Jacobi, S., M., and Schall, J., D. (2004). Dissociation of spatial attention and saccade preparation. Proc. Natl. Acad Sci. U S A. *101*, 15541–15544.

Katz, L.N., Yates, J.L., Pillow, J.W., and Huk, A.C. (2016). Dissociated functional significance of decision-related activity in the primate dorsal stream. Nature *535*, 285–288.

Law, C.-T., and Gold, J.I. (2008). Neural correlates of perceptual learning in a sensory-motor, but not a sensory, cortical area. Nat. Neurosci. *11*, 505–513.

Lo, C.C., Boucher, L., Paré, M., Schall, J.D., and Wang, X.J. (2009). Proactive inhibitory control and attractor dynamics in countermanding action: a spiking neural circuit model. J. Neurosci. *29*, 9059–9071.

Logan, G.D., and Cowan, W.B. (1984). On the ability to inhibit thought and action: a theory of an act of control. Psychol. Rev. *91*, 295–327.

Logan, G.D., Van Zandt, T., Verbruggen, F., and Wagenmakers, E.J. (2014). On the ability to inhibit

thought and action: general and special theories of an act of control. Psychol. Rev. *121*, 66–95.

Logan, G.D., Yamaguchi, M., Schall, J.D., and Palmeri, T.J. (2015). Inhibitory control in mind and brain 2.0: blocked-input models of saccadic countermanding. Psychol. Rev. *122*, 115–147.

Marder, E., Goeritz, M.L., and Otopalik, A.G. (2015). Robust circuit rhythms in small circuits arise from variable circuit components and mechanisms. Curr. Opin. Neurobiol. *31*, 156–163.

Mazurek, M.E., Roitman, J.D., Ditterich, J., and Shadlen, M.N. (2003). A role for neural integrators in perceptual decision making. Cereb. Cortex *13*, 1257–1269.

Middlebrooks, P.G., and Schall, J.D. (2014). Response inhibition during perceptual decision making in humans and macaques. Atten. Percept. Psychophys. *76*, 353–366.

Murthy, A., Ray, S., Shorter, S.M., Schall, J.D., and Thompson, K.G. (2009). Neural control of visual search by frontal eye field: effects of unexpected target displacement on visual selection and saccade preparation. J. Neurophysiol. *101*, 2485–2506.

O'Connell, R.G., Shadlen, M.N., Wong-Lin, K., and Kelly, S.P. (2018). Bridging neural and computational viewpoints on perceptual decision-making. Trends Neurosci. *41*, 838–852.

Paré, M., and Dorris, M. (2011). The role of posterior parietal cortex in the regulation of saccadic eye movements. In Oxford Handbook of Eye Movements, S. Liversedge, I. Gilchrist, and S. Everling, eds. (OUP Oxford), pp. 257–278.

Paré, M., and Hanes, D.P. (2003). Controlled movement processing: superior colliculus activity associated with countermanded saccades. J. Neurosci. *23*, 6480–6489.

Pouget, P., Stepniewska, I., Crowder, E., A., Leslie, M., W., Emeric, E., E., Nelson, M., J., and Schall, J., D. (2009). Visual and motor connectivity and the distribution of calcium-binding proteins in macaque frontal eye field: implications for saccade target selection. Front Neuroanat *3*, 2.

Purcell, B.A., Heitz, R.P., Cohen, J.Y., Schall, J.D., Logan, G.D., and Palmeri, T.J. (2010). Neurally constrained modeling of perceptual decision making. Psychol. Rev. *117*, 1113–1143.

Purcell, B.A., Schall, J.D., Logan, G.D., and Palmeri, T.J. (2012). From salience to saccades: multiple-alternative gated stochastic

accumulator model of visual search. J. Neurosci. *32*, 3433–3446.

Ratcliff, R., Cherian, A., and Segraves, M.A. (2003). A comparison of macaque behavior and superior colliculus neuronal activity to predictions from models of two choice decisions. J. Neurophysiol. *90*, 1392–1407.

Ratcliff, R., Smith, P.L., Brown, S.D., and McKoon, G. (2016). Diffusion decision model: current issues and history. Trends Cogn. Sci. *20*, 260–281.

Roitman, J.D., and Shadlen, M.N. (2002). Response of neurons in the lateral intraparietal area during a combined visual discrimination reaction time task. J. Neurosci. *22*, 9475–9489.

Schall, J.D. (2015). Visuomotor functions in the frontal lobe. Annu. Rev. Vis. Sci. *1*, 469–498.

Schall, J.D. (2019). Accumulators, neurons, and response time. Trends Neurosci. *42*, 848–860.

Thompson, K., G., Biscoe, K., L., and Sato, T., R. (2005). Neuronal basis of covert spatial attention in the frontal eye field. J. Neurosci *25*, 9479–9487.

Verbruggen, F., and Logan, G.D. (2009). Models of response inhibition in the stop-signal and stop-change paradigms. Neurosci. Biobehav. Rev. *33*, 647–661.

Verbruggen, F., and Logan, G.D. (2015). Evidence for capacity sharing when stopping. Cognition *142*, 81–95.

Verbruggen, F., Aron, A.R., Band, G.P., Beste, C., Bissett, P.G., Brockett, A.T., Brown, J.W., Chamberlain, S.R., Chambers, C.D., Colonius, H., et al. (2019). A consensus guide to capturing the ability to inhibit actions and impulsive behaviors in the stop-signal task. Elife. https://doi.org/10.7554/eLife.46323.

Wardak, C., Ibos, G., Duhamel, J.R., and Olivier, E. (2006). Contribution of the monkey frontal eye field to covert visual attention. J. Neurosci. *26*, 4228–4235.

Wei, W., and Wang, X.J. (2016). Inhibitory control in the cortico-basal ganglia-thalamocortical loop: complex regulation and interplay with memory and decision processes. Neuron *92*, 1093–1105.

Xu, K.Z., Anderson, B.A., Emeric, E.E., Sali, A.W., Stuphorn, V., Yantis, S., and Courtney, S.M. (2017). Neural basis of cognitive control over movement inhibition: human fMRI and primate electrophysiology evidence. Neuron *96*, 1447–1458.

Supplemental Information

Countermanding Perceptual Decision-Making

Paul G. Middlebrooks, Bram B. Zandbelt, Gordon D. Logan, Thomas J. Palmeri, and Jeffrey D. Schall

SUPPLEMENTAL INFORMATION

TRANSPARENT METHODS

Experimental Model and Subject Details

All experimental procedures were in accordance with the National Institutes of Health Guide for the Care and Use of Laboratory Animals, the Society for Neuroscience Guidelines and Policies, and approved by the Vanderbilt University Institutional Animal Care and Use Committee.

Nonhuman Primates

Combined neural and performance data were collected from two macaques (82 sessions from M. radiata, male, 7.4 kg, 7 yrs old at the time of data collection, identified as Br; 18 sessions M. radiata, male, 11 kg, 7 yrs old at the time of this data collection, identified as Jo). Performance data only were collected from two macaques (15 sessions from M. mulatta, female, 5.4 kg, 6 yrs old at the time of this data collection, identified as X; 15 sessions from Br).

Method details

Surgical preparation

Monkeys were surgically implanted with Crist CILUX recording chambers over FEF under aseptic conditions with isoflurane anesthesia. Antibiotics and analgesics were administered postoperatively. A craniotomy was made, allowing recording access to the periarcuate area, and a headpost was affixed to the skull via ceramic screws. Monkeys were allowed 6 weeks to recover following surgery before being placed back on task.

Neural and performance data acquisition

Monkeys sat comfortably with head restrained in a primate chair, facing a computer display (46° x 36° visual angle, 70 Hz refresh rate) in a darkened room. Stimulus presentation, reward delivery, and task contingences were controlled by TEMPO/VIDEOSYNC software (Reflective Computing). Eye position was digitized (1 kHz, Eyelink 1000, SR Research) and streamed to a data acquisition system (Plexon). Fluid reinforcement was delivered with a solenoid-operated gravity-flow system.

Neuronal spiking was recorded from macaque Br using various electrodes (47 sessions using single tungsten electrodes, 13 sessions using multi-channel (8 or 24) U-Probe vector arrays, and 19 sessions using 32-channel Neuronexus vector arrays). Data were collected from Jo over 18 sessions using 32-channel Neuronexus vector arrays. Neurons were considered task-modulated if their spike rates varied as a function of visual stimuli and/or eye movements. From Br were sampled 551 modulated neurons; from Jo, 376. If electrode drift compromised isolation, all neurons on each electrode channel were combined for analyses,

which provided stable estimates of spike rates. We tested the validity of this approach by comparing analysis outcomes for well-isolated spikes and the multi-unit combination. None of the conclusions change.

Neural localization

Structural MR images were acquired to guide placement of recording chambers with a Philips Intera Achieva 3 tesla scanner using SENSE Flex-S surface coils placed above and below the head. T1-weighted gradient-echo structural images were obtained with a 3D turbo field echo anatomical sequence (TR = 8.729 ms; 130 slices, 0.70 mm thickness). Recordings were localized in the arcuate sulcus using high-resolution MR imaging. A grid placed in the recording chamber was filled with Magnevist, and whole brain structural images were acquired with a T1 weighted MPRAGE sequence (TR/TE = 9.3/4.6 ms), isometric voxel resolution of 0.5 mm. High resolution T1-weighted spin echo images (TR/TE = 1625/18 ms) were acquired with an isometric in-plane resolution of 0.25 mm and slice thickness of 1 mm. We acquired eight volumes, four oriented orthogonal to the grid holes and four, parallel. The images were co-registered to a reference template of the individual monkey in stereotaxic coordinates. An MR representation of the grid was obtained by averaging slices across grid depths. Spikes were assigned to location in the arcuate based on the projection of the grid into the brain.

Perceptual decision countermanding task

Monkeys earned fluid reward for shifting gaze to one of two targets according to the dominant color of a choice stimulus unless a stop signal appeared, in which case they earned reward for canceling the planned saccade. Trials began when monkeys fixated a spot (0.5˚ square) in the center of the display (Figure 1A). After a variable duration (400-800 ms), two targets (1° square) appeared in the periphery, one in each hemifield (8-15° eccentricity). Monkeys maintained fixation for a variable duration (400-800 ms) until the fixation spot was extinguished. Simultaneously, the choice stimulus appeared (1˚ square 3° above fixation) consisting of 10x10 square checkerboard with randomly assigned isoluminant (30 cd/m^2 on 13 cd/m^2 gray background) cyan and magenta squares (magnified inset in Figure 1). The assignment of cyan or magenta to leftward or rightward responses was counterbalanced across monkeys. Discriminability varied according to color coherence, which was set to 4 values during neural recording sessions. Color coherence values were adjusted separately for each monkey, with sign distinguishing rewarded direction assigned to color (Br ±8%, ±3; Jo ±10%, ±5%). Saccade RT was the duration between presentation of the choice stimulus and eye velocity exceeding 30˚/sec; RT > 1000 ms were unrewarded but vanishingly rare.

The stop signal was presented on a random ~1/3 of trials (30-45%, adjusted to maximize yield of informative trials), consisting of re-appearance of the fixation spot after a variable stop-signal delay (SSD). To equilibrate proportions of canceled and noncanceled stop trials, SSD was adjusted using a staircase procedure within color coherence, increasing after a canceled stop trial and decreasing after a noncanceled stop trial. SSD was adjusted in random steps of 1, 2 or 3 intervals, consisting of 1-7 video frames (70 Hz refresh rate). Step intervals were constant within but could vary across sessions. Reward was delivered on stop signal trials after monkeys maintained gaze on the fixation spot for 1500 ms.

A saccade to the incorrect target on no-stop trials or a saccade to either target on stop signal trials resulted in a brief timeout. A saccade to the choice stimulus at any time aborted the trial and resulted in a brief timeout. Aborts were rare (Br behavioral sessions: 1.6%; X behavioral sessions: 0.6%; Br neural recording sessions: 2.0%; Jo neural recording sessions: 1.6% of all trials). After receiving reward or timeouts, monkeys experienced a 1 second inter-trial interval.

Stochastic accumulator model

We extended the interactive race model of countermanding (Boucher et al. 2007; Logan et al. 2015) to incorporate two-alternative decision-making. The model included three stochastic accumulators. One GO unit accumulates evidence for one color (GO⁺); another, for the other color (GO⁻), according to color coherence (COH). Three interactions between the GO units were evaluated: race, lateral inhibition, and feedforward inhibition. During simulated no-stop-signal trials, color choice and RT were specified when the first GO unit reached threshold. During simulated stop-signal trials a STOP unit was activated after stop-signal presentation and inhibited both GO units when it reached threshold. Simulated canceled trials occurred if the STOP unit prevented either GO unit from accumulating to threshold. Simulated non-canceled trials occurred if either GO unit reached threshold. The dynamics of GO and STOP unit activation within a trial were governed by these equations:

$$da_{GO}^+(t) = \frac{dt}{\tau}\left[\mu_{GO}^+(COH) - \left(u \cdot \mu_{GO}^-(COH)\right) - \left(\beta_{GO} \cdot a_{GO}^-(t)\right) - \left(\beta_{STOP} \cdot a_{STOP}(t)\right) - \left(k_{GO} \cdot a_{GO}^+(t)\right)\right] + \sqrt{\frac{dt}{\tau}}\xi$$

$$da_{GO}^-(t) = \frac{dt}{\tau}\left[\mu_{GO}^-(COH) - \left(u \cdot \mu_{GO}^+(COH)\right) - \left(\beta_{GO} \cdot a_{GO}^+(t)\right) - \left(\beta_{STOP} \cdot a_{STOP}(t)\right) - \left(k_{GO} \cdot a_{GO}^-(t)\right)\right] + \sqrt{\frac{dt}{\tau}}\xi$$

$$da_{STOP}(t) = \frac{dt}{\tau}\left[\mu_{STOP} - k_{STOP} \cdot a_{STOP}(t)\right] + \sqrt{\frac{dt}{\tau}}\xi$$

The activation of each GO unit (a_{GO}) increased with input strength, which varied with color coherence and response direction ($\mu_{GO}(COH_i)$) and could decrease according to feedforward inhibition (u) scaled by the input strength to the other GO unit, by lateral inhibition (β_{GO}) scaled by the current activation of the other GO unit, by STOP unit inhibition (β_{STOP}) scaled by the current activation of the STOP unit, and by leak proportional to activation (k_{GO}). For the race architecture $u = \beta_{GO} = 0$. For the feedforward inhibition architecture $u > 0$, $\beta_{GO} = 0$. For the lateral inhibition architecture $u = 0$, $\beta_{GO} > 0$. The activation of the STOP unit (a_{STOP}) increased with input strength (μ_{STOP}) and decreased according to leak proportional to activation (k_{STOP}). Gaussian noise (ξ) was added to the deterministic activation of each unit. Activation of units began at a baseline level on each trial

drawn from a uniform distribution [0:A_0], which could have different values for the GO$^+$ and GO$^-$ units, accounting for response biases, and for the STOP unit. Activation completed when reaching the respective thresholds (A_{θ_GO}, A_{θ_STOP}). Activation of each unit began after a non-decision time (t_0) accounting for the duration of stimulus encoding, which could have different values for the GO and STOP units.

Models were fit by minimizing the chi-square statistic using the Nelder-Mead simplex algorithm in MATLAB. Goodness of fit was assessed using the BIC statistic:

$$\mathrm{BIC} = -2\left[\sum_i \mathrm{N} \cdot \mathrm{p_i} \cdot \ln(\pi_i)) + \mathrm{M} \cdot \ln(\mathrm{N})\right]$$

where p_i and π_i are the proportions of observed and predicted data in the ith bin, N is the number of observations in the condition, and M is the number of free parameters in the model.

Quantification and statistical analysis
All analyses were performed using MATLAB (MathWorks, Natick, MA).

Performance analyses
Each monkey provided multiple data collection sessions, so behavioral analyses throughout the study were performed within-subjects, across sessions. Choice accuracy was characterized in psychometric plots of the P(rightward saccade) as a function of the percentage of rightward color coherence. Psychometric functions were fit with a Weibull curve using maximum likelihood methods. Choice RT was characterized in chronometric plots of RT as a function of color coherence. To compare stopping performance across choice difficulty, SSRT was estimated within color coherence levels. Given the large number of experimental conditions, we obtained at least 50 stop-signal trials per color coherence per session. SSRT was calculated using the integration method (Verbruggen et al. 2013).

Neural analyses
Neurons were classified based on their response properties during task. For this study, we focused on two types of neurons in FEF. Movement neurons increased discharge rates before saccade initiation, i.e., spike rates 50 ms before the saccade exceeded those during 300 ms before the targets appeared (paired t-test). Visuo-movement neurons paralleled movement neurons before saccades with additional modulation 50-125 ms after visual target presentation (paired t-test). Movement fields (MF) were defined as the direction that elicited the highest presaccadic spike rates.

To determine whether unit spiking represented a decision variable, we measured the variation of discharge rate as a function of saccade direction and color coherence. A neuron contributed to the decision if discharge rate varied with color coherence for choices into the MF and either did not vary or varied in opposite sign for choices out of the MF (Ding and Gold 2011). Spike rates were measured in spike density functions (SDF) obtained by convolving individual spike trains with a kernel with the timing characteristics of an excitatory post-

synaptic potential (Thompson et al. 1996). To test whether a unit varied by response direction, we compared discharge rates between the choice stimulus and saccade initiation between no-stop trials with responses into versus out of MF using a Wilcoxon rank sum test. To test whether a unit varied by color coherence, we compared mean SDFs during the decision epoch between easy and hard color coherence levels, within response direction.

To determine whether unit spiking contributed to response inhibition, we measured the modulation of discharge rate on canceled trials compared to RT-matched no-stop trials (Hanes et al. 1998). A neuron contributed to response inhibition if discharge rate on canceled trials was significantly different from that on no-stop trials before SSRT. Comparisons were made within each SSD x color coherence condition having ≥10 trials with SDF aligned on choice stimulus presentation. The mean SDF of canceled stop trials was subtracted from the mean SDF of RT-matched no-stop trials. This difference was judged significant if it exceeded by at least 2 standard deviations, for at least 75 ms, the average difference measured for the same trials in the 500 ms before choice stimulus presentation. Cancel time was defined as the time of a significant difference in magnitude and trajectory relative to the session SSRT. A neuron was classified as contributing to response inhibition if it canceled within 40 ms of SSRT for the session. To provide comparable measurements for simulated GO unit trajectories, the same procedure and criterion was used.

References

Thompson, K.G., Hanes, D.P., Bichot, N.P., Schall, J.D. Perceptual and motor processing stages identified in the activity of macaque frontal eye field neurons during visual search. J Neurophysiol. 1996; 76: 4040-4055.

Verbruggen, F., Chambers, C.D., Logan, G.D. Fictitious inhibitory differences: how skewness and slowing distort the estimation of stopping latencies. Psychol Sci. 2013; 24: 352-362.

Br neural recording

		Color Coherence (%)			
		-8	-3	3	8
No stop	Number of trials	840	771	778	808
	Correct choice RT	544 (8)	571 (13)	457 (13)	352 (6)
	Error choice RT	614 (50)	540 (51)	601 (20)	679 (83)
Noncanceled	Number of trials	303	260	276	314
	Correct choice RT	479 (8)	522 (9)	383 (7)	308 (6)
	Error choice RT	432 (98)	473 (34)	513 (60)	442 (73)
Canceled	Number of trials	308	267	279	310
	SSRT	66 (23)	57 (16)	46 (19)	63 (14)

Jo neural recording

		Color Coherence (%)			
		-10	-5	5	10
No stop	Number of trials	347	320	319	335
	Correct choice RT	273 (3)	310 (7)	426 (11)	379 (11)
	Error choice RT	451 (86)	455 (40)	326 (10)	331 (25)
Noncanceled	Number of trials	334	319	317	333
	Correct choice RT	261 (2)	283 (3)	333 (14)	309 (6)
	Error choice RT	263 (47)	322 (30)	299 (10)	323 (52)
Canceled	Number of trials	1128	1092	1134	1139
	SSRT	81 (20)	76 (26)	89 (15)	96 (24)

Br behavior only

		Color Coherence (%)					
		-7	-5	-3	3	5	7
No stop	Number of trials	2502	2868	3357	3290	2749	2290
	Correct choice RT	337 (12)	368 (13)	386 (12)	428 (11)	392 (9)	363 (8)
	Error choice RT	456 (104)	457 (72)	461 (45)	388 (63)	387 (73)	357 (53)
Noncanceled	Number of trials	836	980	1116	1075	896	729
	Correct choice RT	294 (9)	311 (10)	325 (12)	356 (8)	337 (6)	309 (6)
	Error choice RT	343 (131)	353 (65)	363 (45)	314 (42)	300 (48)	308 (77)
Canceled	Number of trials	824	966	1116	1073	888	721
	SSRT	65 (12)	66 (21)	61 (14)	71 (23)	74 (18)	86 (15)

X behavior only

		Color Coherence (%)					
		-15	-8	-3	3	8	15
No stop	Number of trials	1564	1575	1522	1530	1572	1487
	Correct choice RT	307 (8)	351 (9)	323 (9)	293 (6)	287 (4)	278 (5)
	Error choice RT	281 (41)	300 (49)	293 (24)	325 (34)	331 (46)	358 (100)
Noncanceled	Number of trials	504	510	473	502	495	479
	Correct choice RT	283 (9)	288 (7)	292 (8)	272 (6)	269 (4)	269 (7)
	Error choice RT	251 (29)	254 (23)	270 (19)	290 (28)	311 (89)	312 (84)
Canceled	Number of trials	517	531	493	487	508	496
	SSRT	65 (32)	54 (20)	60 (26)	78 (58)	71 (34)	88 (61)

Table S1. Perceptual decision countermanding performance. Related to Figure 1.
Shown are the number of trials (N) and average (SEM) response time for the indicated types of trials for the 4 sets of data. A total of four performance data sets were collected, two during neural data collection (Br, Jo), a third from monkey Br before neural recordings, and the fourth from a third monkey (X). Color coherence values were adjusted separately for each monkey and dataset (Br during neural recordings ±8%, ±3; Jo during neural recordings ±10%, ±5%; Br behavior only ±7%, ±5%, ±3; X behavior only ±15%, ±8%, ±3%). Macaque Br performed 82 neural recording sessions yielding 101,683 trials (mean = 1,240 trials/session). Macaque Jo performed 18 neural recording sessions yielding 29,621 trials (mean = 1,646 trials/session. Of the neural recording sessions, 5 sessions each were chosen from Br and Jo for modeling, based on quality of behavioral performance and near equality of trials from each monkey. Macaque Br also performed 15 behavioral sessions yielding 33,258 trials (mean = 2,217 trials/session). Macaque X performed 15 behavioral sessions yielding 25,927 trials (mean = 1,729 trials/session).
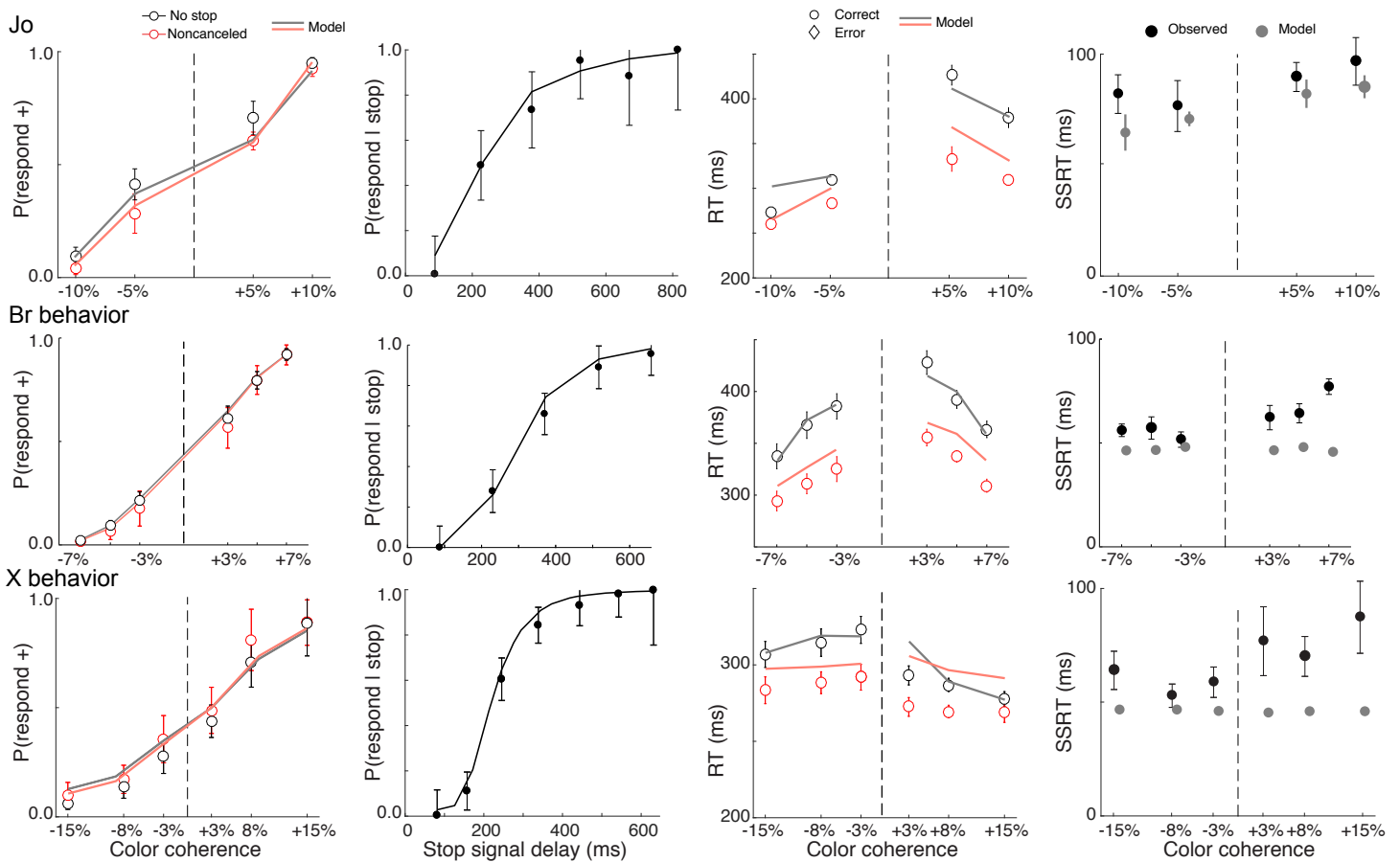
Figure S1. Perceptual decision countermanding performance. Related to Figure 1.
Summary of performance from monkey Jo during neural recordings (top), Br behavior only (middle), and X behavior-only (bottom). **First column,** Mean ± SEM probability of choosing the positive color no stop (black) and non-canceled (red) trials. Some standard error bars are smaller than the symbols. Discriminability varied with color coherence, which was set to 4 values during neural recording sessions and to 6 values during performance testing alone. Best model fits are shown for no stop (gray) and non-canceled (red) trials. **Second column,** Mean ± SEM inhibition functions. The variation of response inhibition with stop-signal delay predicted by the best-fitting model is plotted (solid line). **Third column,** Mean ± SEM of response time (RT) as a function of color coherence for correct choice no-stop (black) and noncanceled (red) trials. Response times and error rate increased significantly with difficulty (Br behaviour only: RT: $F_{(5,329)} = 5.63$, $\eta_p^2 = 0.08$, $p < 0.001$; Accuracy: $F_{(5,173)} = 1284$, $\eta_p^2 = 0.49$, $p < 0.001$; X: RT: $F_{(5,332)} = 2.18$, $\eta_p^2 = 0.03$, $p = 0.056$; Accuracy: $F_{(5,173)} = 316$, $\eta_p^2 = 0.47$, $p < 0.001$). Noncanceled RT was systematically shorter than no-stop RT, justifying the application of the Logan race model. Best model fits are shown for no stop (gray) and non-canceled (red) trials. **Fourth column,** Mean ± SEM stop-signal reaction time (SSRT) derived from the race model as a function of color coherence. SSRT did not vary systematically with choice difficulty (Br-behavioral: $F_{(5,84)} = 3.67$, $\eta_p^2 = 0.18$, $p = 0.005$; X-behavioural: $F_{(5,84)} = 1.26$, $\eta_p^2 = 0.07$, $p = 0.29$). Mean and range of SSRT from best model fits are shown (gray).
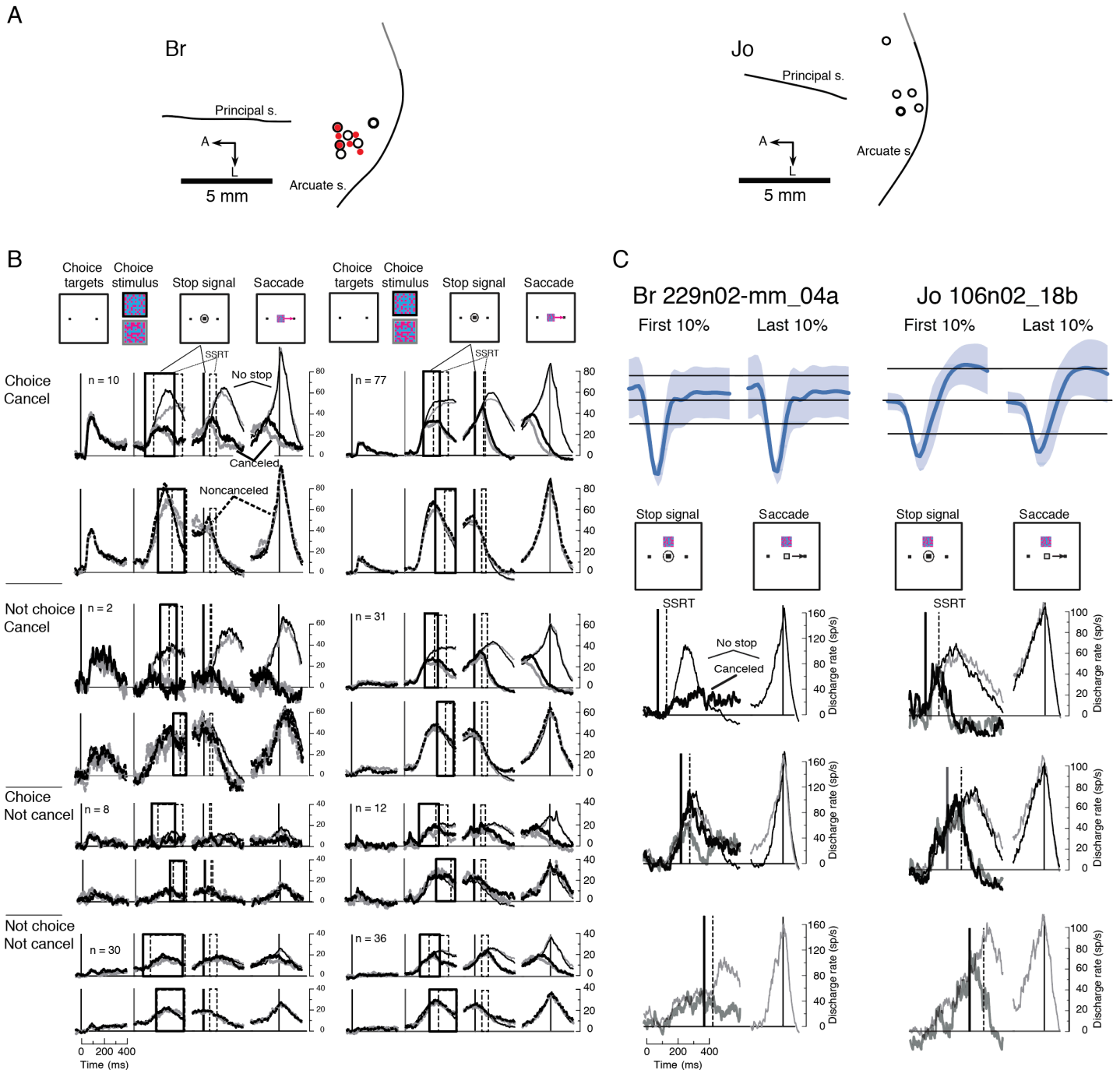
Figure S2. Characteristics of neural activity. Related to Figure 2.
(A) Open circles mark sites where neurons were sampled in multiple penetrations. Red dots mark sites where saccades were elicited with intracortical electrical microstimulation with currents <50 µA. Neurons were sampled in the FEF on the rostral bank of the arcuate sulcus caudal and lateral to the principal sulcus.

(B) Neuron samples from monkey Br (left) and Jo (right). The average discharge rate of neuron samples is plotted in a quartet of plots comparing activity on canceled trials (thick solid) with activity on latency-matched no stop signal trials (thin solid) (top quartet) and comparing activity on noncanceled trials (thick dotted) with activity on latency-matched no stop signal trials (thin solid) (bottom quartet). Neural activity on trials with an easier discrimination is plotted in black. Neural activity on trials with difficult discrimination is plotted in gray. Within a quartet, average discharge rate is plotted aligned on presentation of the choice targets (first panel), discrimination stimulus (second panel), stop signal (third panel), and saccade (fourth panel). In the second and

third panels the thick rectangle or line indicates the range of stop signal presentation times, and the dashed rectangle bounds the consequent range of SSRT. For each monkey, the **top** set of plots shows the average discharge rate of neurons modulated by choice difficulty and exhibiting the countermanding cancel signal. In both monkeys many neurons were found that signaled choice difficulty, evident by the lack of overlap of the black and gray discharge rate in the second panel, and also modulated before SSRT when saccades were canceled but did not modulate on noncanceled trials, evident by the overlap of discharge rate associated with the saccade. The **second** set of plots shows the average discharge rate of neurons not modulated by choice difficulty but exhibiting the countermanding cancel signal. Most likely, the difference in discharge rate across choice difficulty just failed to reach statistical significance due to low trial count per neuron or displacement of the choice targets from the most sensitive location of neuron response field, which was evident in the absence of response to the choice targets in monkey Jo. The **third** set of plots shows the average discharge rate of neurons modulated by choice difficulty but not exhibiting the countermanding cancel signal. FEF neurons that modulate on canceled trials after SSRT have been observed previously. The **bottom** set of plots shows the average discharge rate of neurons not modulated by choice difficulty or modulating before SSRT. The absence of difference across choice difficulty appears to be due to the displacement of the choice targets from the most sensitive location of neuron response field, which was evident in the absence of response to the choice targets in monkeys Br and Jo. As noted, FEF neurons that modulate on canceled trials after SSRT have been observed previously. The natural variation of modulation patterns observed previously was replicated here.

(C) Representative single units representing the perceptual decision variable and instantiating race model GO process recorded from Br (left) and Jo (right). Top panels illustrate spike waveforms from the first 10% and the last 10% of trials in each session. Stability of isolation is confirmed by the consistency of waveshapes. The panels below plot baseline corrected average discharge rates for each neuron on trials with no stop signal (thin) and on successfully canceled stop signal trials (thick), aligned on presentation of the stop signal at successively longer SSD (left) and on initiation of the saccade (right). Trials with high (black) and lower (grey) color coherence are distinguished. Representation of the decision variable is evident in the lower discharge rate and slower accumulation in the trials with the lower relative to the higher color coherence. Instantiation of the race model GO process is evident in the pronounced inhibition of discharge rate within SSRT when saccades were canceled. The longest SSD for both monkeys includes only trials with low color coherence because only they have RT longer than SSD + SSRT. This consequence of sampling RT distributions is further evidence at the single neuron level for countermanding perceptual decision making.

	Br	Jo	Sum
All modulated neurons	374	322	696
Presaccadic modulation	50	156	206
Drift-diffusion modulation	18	89	107
Cancel modulation	12	108	120
Presaccadic $\wedge$ drift-diffusion $\wedge$ cancel	10	77	87

Table S2. Summary of neural properties. **Related to Figure 2**.
Counts of unit recordings meeting the indicated criteria for both monkeys. This analysis focused exclusively on FEF neurons with discharge rates that accumulated to a threshold to produce saccades. The many other neurons with only visual responses to the targets and to the checker stimulus were not relevant for the questions considered here. Presaccadic activity required elevated discharge rate at least 150% over fixation period activity. Modulation consistent with drift-diffusion required discharge rate proportional to color coherence (Wilcoxon signed-rank test). Modulation consistent with the Logan race model required presaccadic discharge rates that were increasing to the trigger threshold to be attenuated within SSRT. In all, 206 presaccadic neurons were sampled. Of these 52% were modulated in parallel to a drift diffusion decision process, and 58% exhibited the countermanding cancel modulation. Of those modulated as the drift diffusion decision process, 81% also exhibited the countermanding cancel modulation.
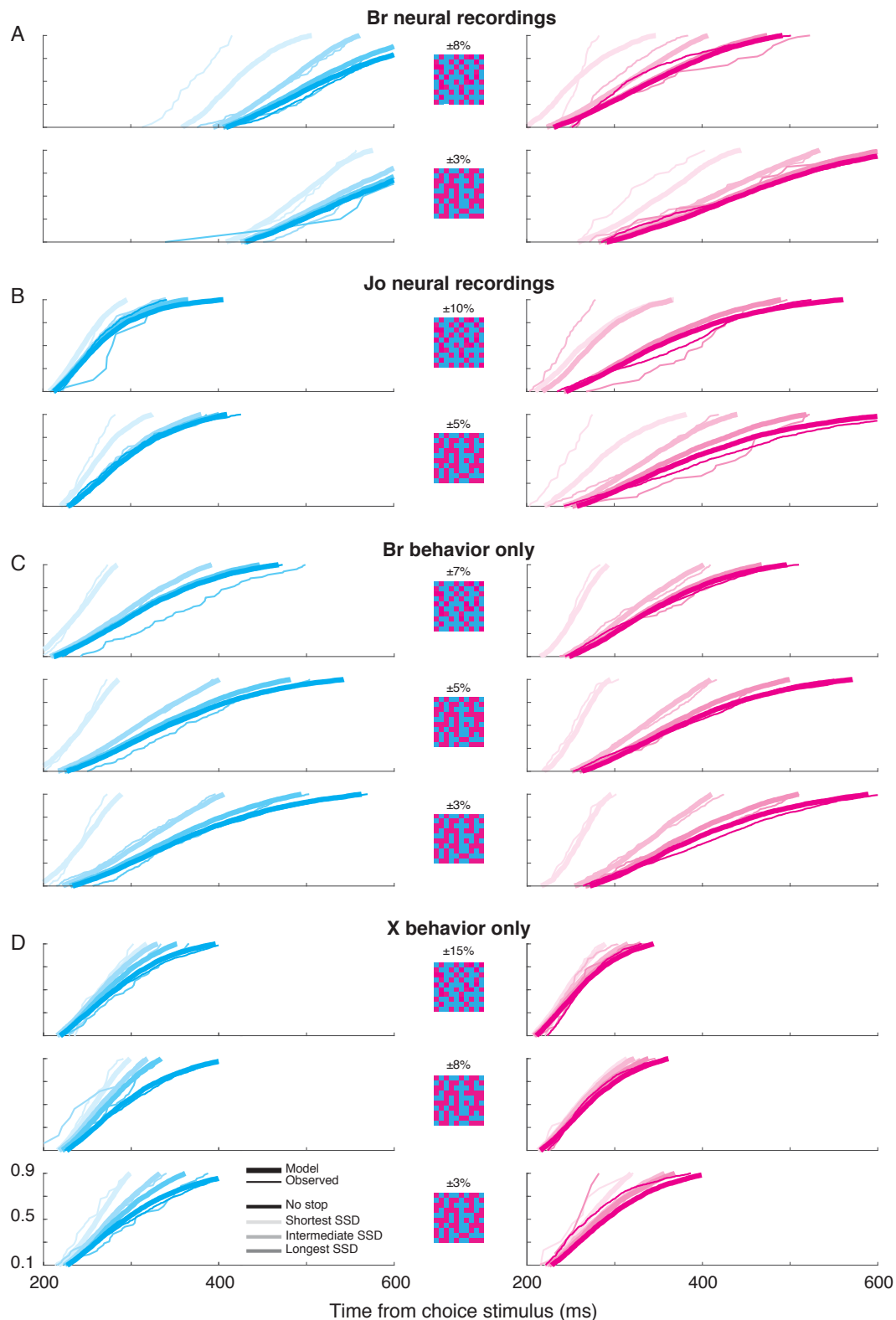
Figure S3. Observed and model RT. Related to Figure 3.
Cumulative distributions of observed (thin) and model (thick) RT to the left and right following presentation of easier (top) or harder (bottom) perceptual choices for no stop (darkest) and non-canceled stop signal trials with progressively longer SSD values (lightest to darkest).
(A) Br performance during neural recordings.
(B) Jo performance during neural recordings.
(C) Br performance before physiology data collection.
(D) X performance.